Supporting Informations for

In Silico and In Cell Hybrid Selection of Nonrapalog Ligands to Allosterically Inhibit the Kinase Activity of mTORC1

Raef Shams[1,2], Akihiro Matsukawa[3], Yukari Ochi[3], Yoshihiro Ito[1,4], and Hideyuki Miyatake[2,4*]

[1] Emergent Bioengineering Materials Research Team, RIKEN Center for Emergent Matter Science, RIKEN, Wako, Saitama 351-0198, Japan

[2] Department of Life Science, Graduate School of Science and Engineering, Saitama University, Saitama city, Saitama 338-8570, Japan

[3] Graduate School of Medicine, Dentistry and Pharmaceutical Sciences, Okayama University, 2-5-1, Shikata, Kita-ku, Okayama, 700-8558 Okayama, Japan

[4] Nano Medical Engineering Laboratory, RIKEN Cluster for Pioneering Research, RIKEN, Wako, Saitama 351-0198, Japan

***Correspondence**: miyatake@riken.jp

Contents of Supporting Informations:

1- Figure S1. Binding mode of rapamycin (RAP) at the FKBP12 and FRB interface.
2- Figure S2. **WRX606** structural conformation by (A) ^{1}H NMR, (B) MALDI-MS and (C) HPLC.
3- Figure S3. FKBP12–**WRX606**–FRB ternary complex.
4- Figure S4. In silico docking models of FKBP12–FRB binding ligands.
5- Figure S5. **WRX601** structural conformation by (A) ^{1}H NMR, (B) MALDI-MS and (C) HPLC.
6- Figure S6. FKBP12–**WRX601**–FRB ternary complex.
7- Figure S7. SMD simulations of FRB/FKBP12 complexes with the first screen ligands.
8- Figure S8. SMD simulations of FRB/FKBP12 complexes with the second screen ligands (part 1).
9- Figure S9. SMD simulations of FRB/FKBP12 complexes with the second screen ligands (part 2).
10- Figure S10. Sequence alignments of FKBP12 or FRB point mutants.
11- Figure S11. Inhibition of mTORC1 by **WRX606**.
12- Figure S12. Cytotoxicity of **WRX606** under feeding-induced activation conditions.
13- Figure S13. Cancer-specific cytotoxicity of **WRX606**.
14- Figure S14. Animal model to assay **WRX606** for organs toxicity.
15- Table S1. Residual interactions of FRB and FKBP12 with rapamycin.
16- Table S2. Characteristics of virtual ligands libraries.
17- Table S3. Prediction results of the selected ligands.
18- Table S4. Residual interactions of FRB and FKBP12 with **WRX606**.
19- Table S5. Residual interactions of FRB and FKBP12 with **WRX513**.
20- Table S6. Residual interactions of FRB and FKBP12 with **WRX939**.
21- Table S7. Residual interactions of FRB and FKBP12 with **WRX601**.

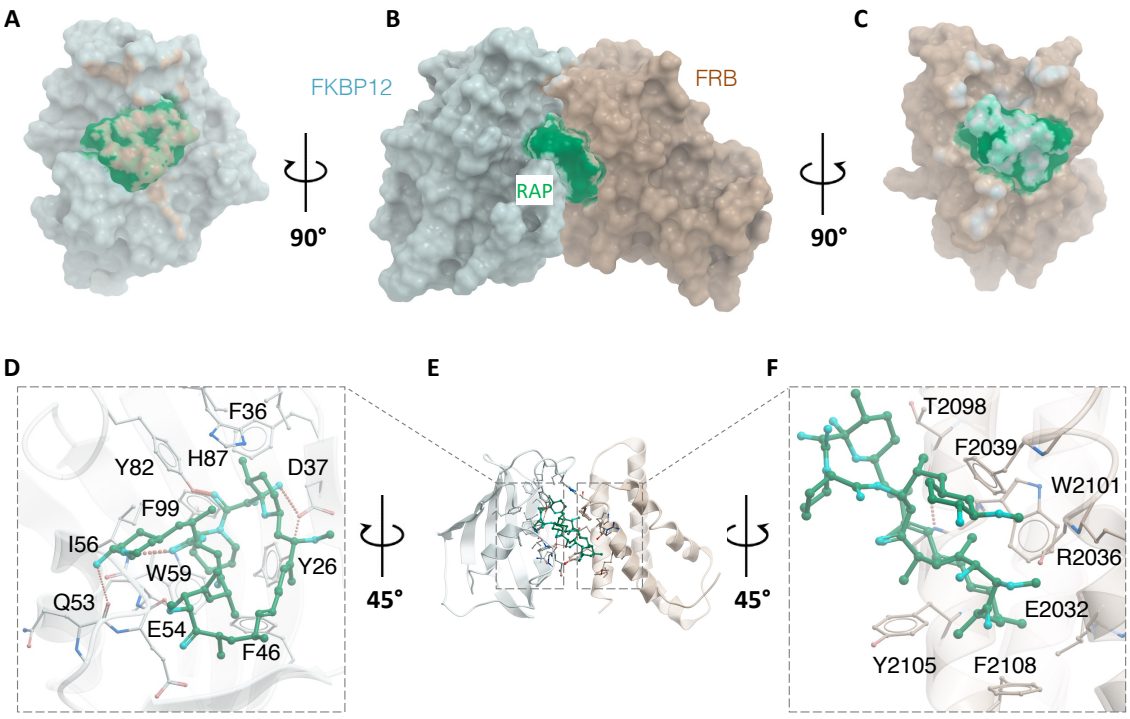

Figure S1. Binding mode of rapamycin (RAP) at the FKBP12 and FRB interface. (A) Molecular surface representations showing rapamycin (green) at the FKBP12 (light blue) canonical groove. (B) Lateral view of FKBP12–RAP–FRB terenary complex (PDB ID: 1FAP). (C) Rapamycin in the FRB (buff) binding site. (D) Close-up view of rapamycin in the ligand-binding site of FKBP12 side with the residues involved in the binding. Red dotted lines represent hydrogen bonds (hydrogen bond between Y26 and D37 for receptor stability). (E) Lateral view of the ternary complex. (F) Close-up view of rapamycin in the ligand-binding site of FRB side with the residues involved in the binding.

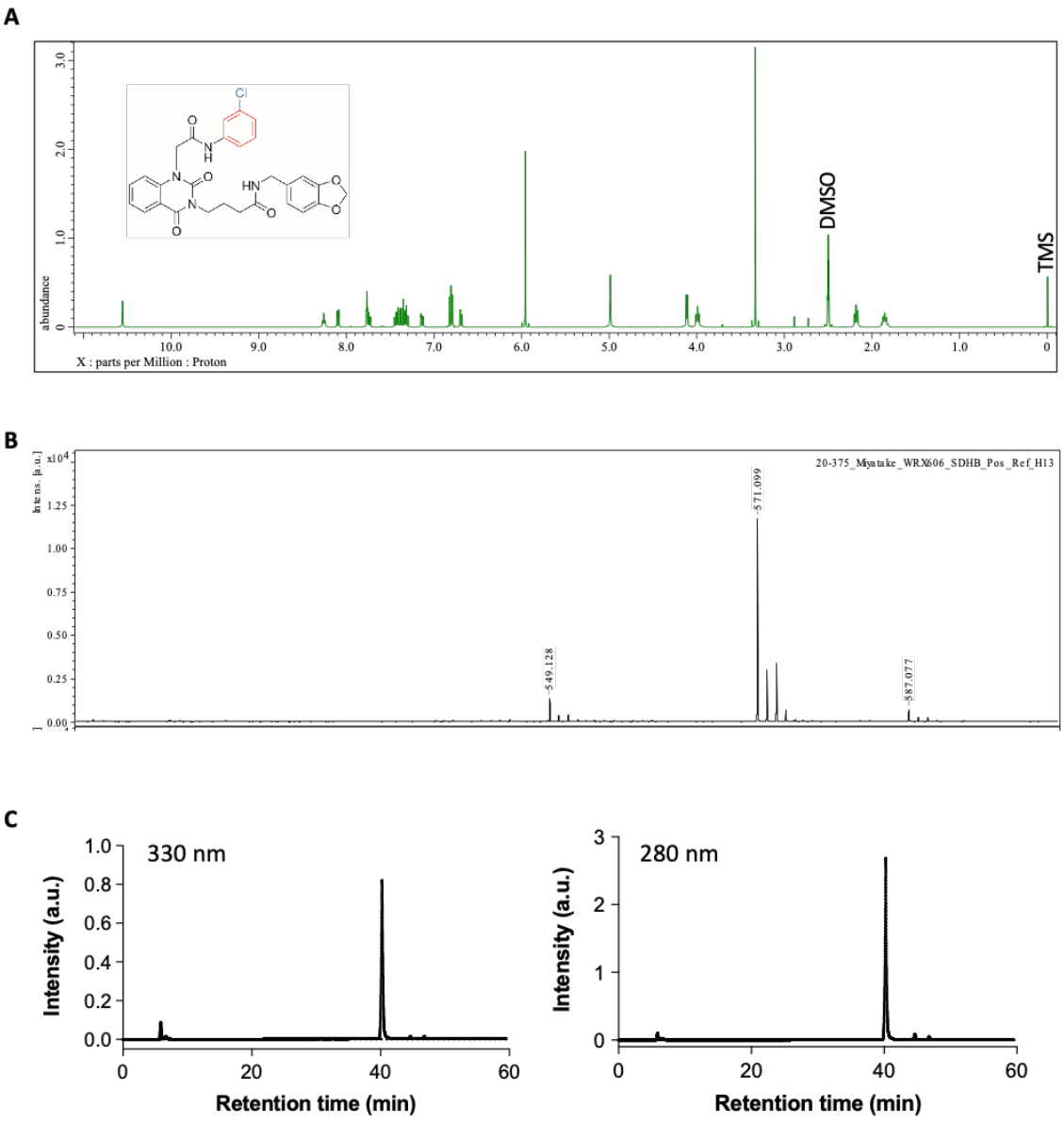

Figure S2. WRX606 structural and purity confirmation by (A) ^{1}H NMR, (B) MALDI-MS and (C) HPLC analysis (Purity >95%).

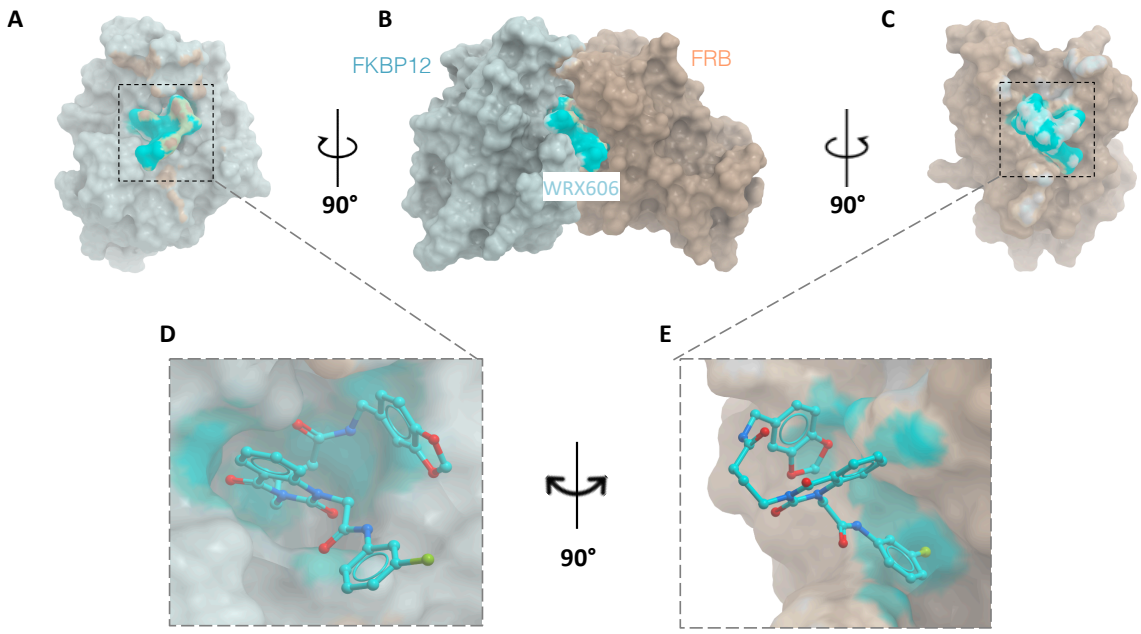

Figure S3. FKBP12–WRX606–FRB ternary complex. (A) Molecular surface representation of **WRX606** (cyan) at FKBP12 binding site (light blue). (B) Lateral view of FKBP12–**WRX606**–FRB ternary complex. (C) **WRX606** in the FRB (buff) binding site. (D) Close-up view of **WRX606** at the FKBP12 binding cleft. (E) Close-up view of **WRX606** at the FRB binding cleft.

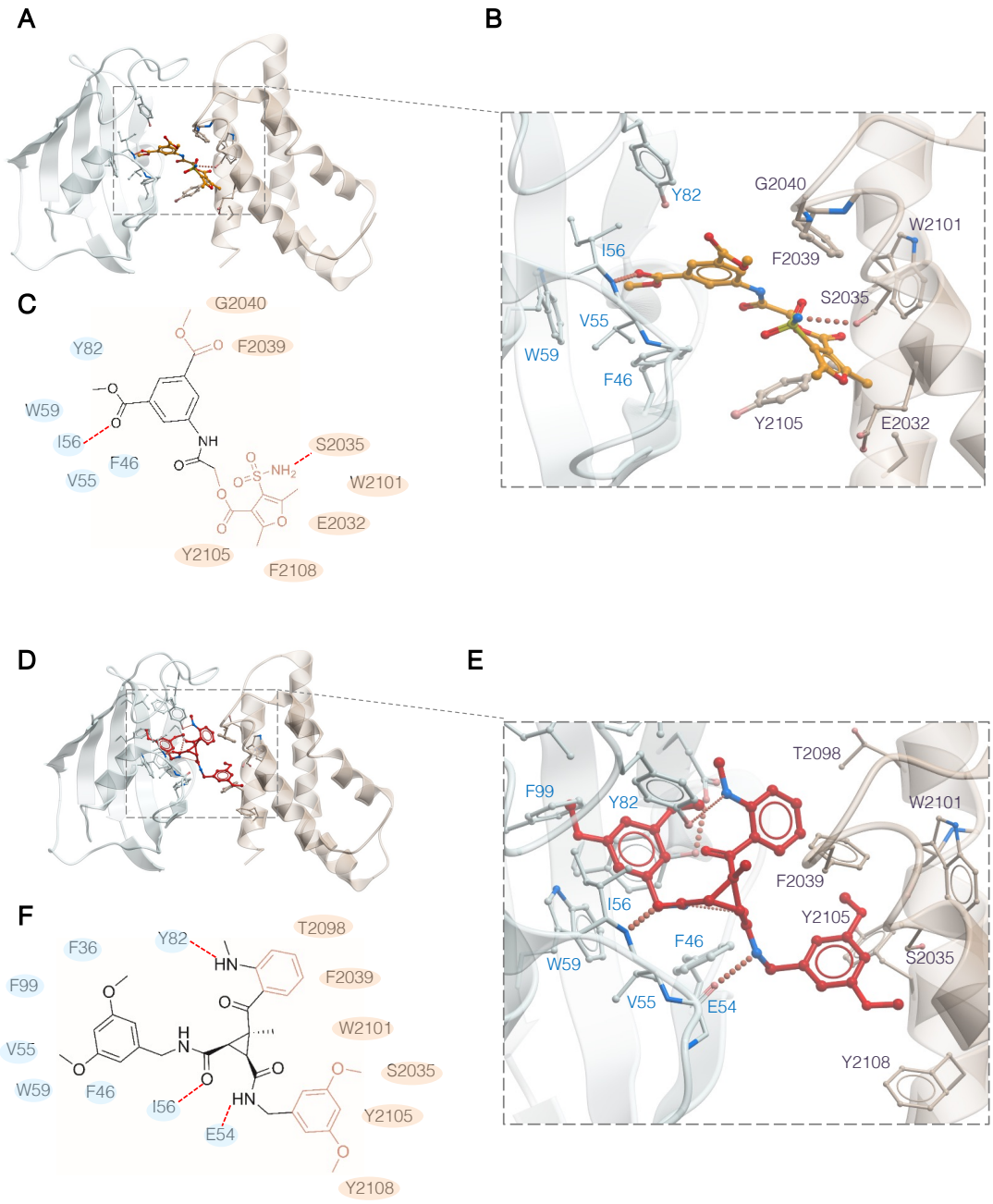

Figure S4. In silico docking models of FKBP12–FRB binding ligands. (A) Lateral view of ZINC 32928513 (**WRX 513** ; orange) at the FKBP 12 (light blue)–FRB (buff) interface shown by ribbon representations . (B) Close -up view of **WRX 513** at the FKBP 12/FRB binding site showing the binding residues . (C) 2D representation of **WRX513** with binding residues. (D) Lateral view of ZINC100492939 (**WRX 939**; red) at the FKBP 12–FRB interface shown by ribbon representations . (E) Close -up view of **WRX 939** at the FKBP 12/FRB binding site showing the binding residues . (F) 2D representation of **WRX939** with binding residues. Residues of the ternary complexes involved in ligand -binding are present . Hydrogen bonds are drawn as dotted lines (red) in the ribbon representations . In the 2D representations , FKBP 12 and FRB residues are highlighted in light blue and light orange, respectively.

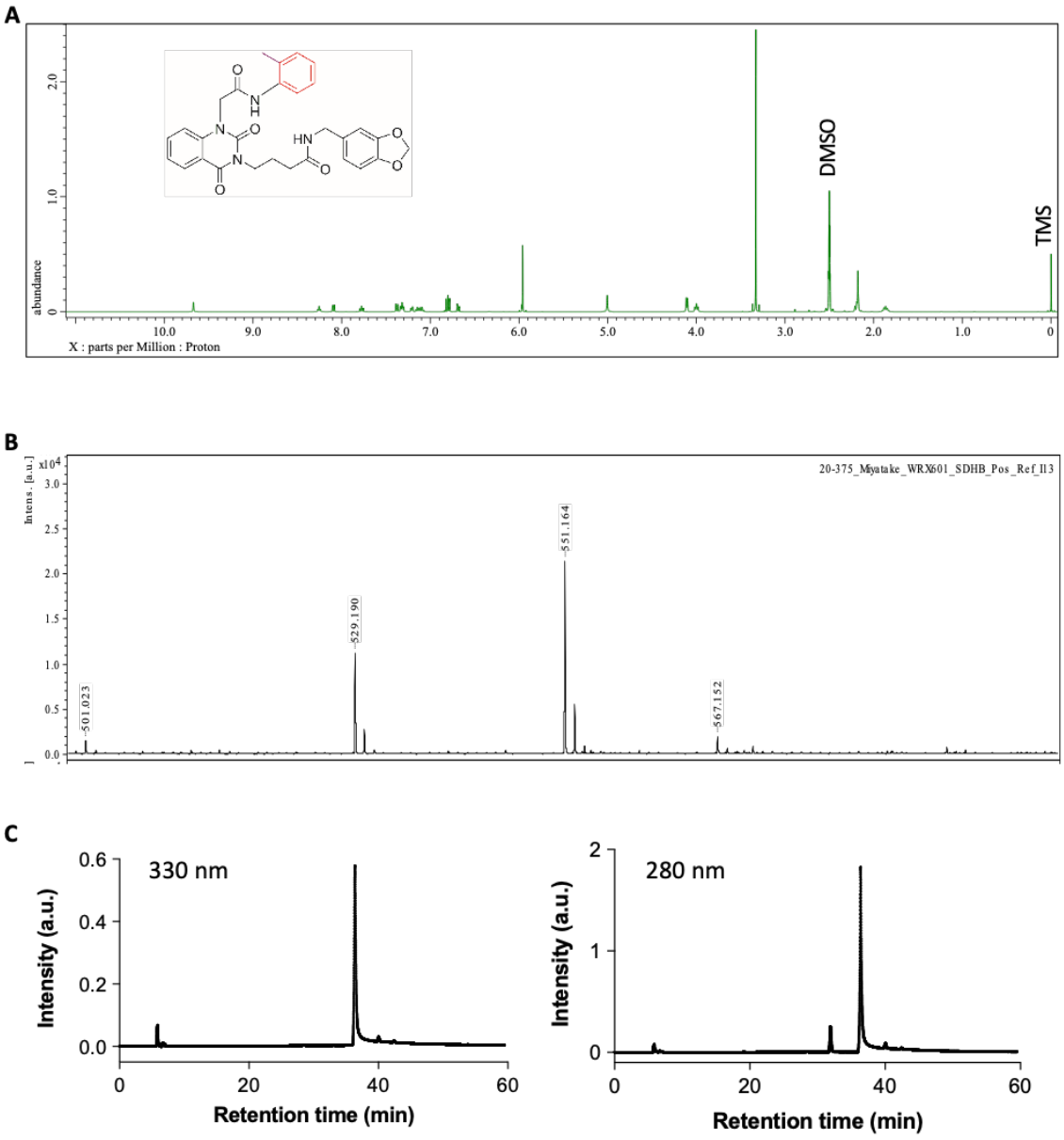

Figure S5. WRX601 structural and purity confirmation by (A) ^{1}H NMR, (B) MALDI-MS and (C) HPLC analysis (Purity > 90%).

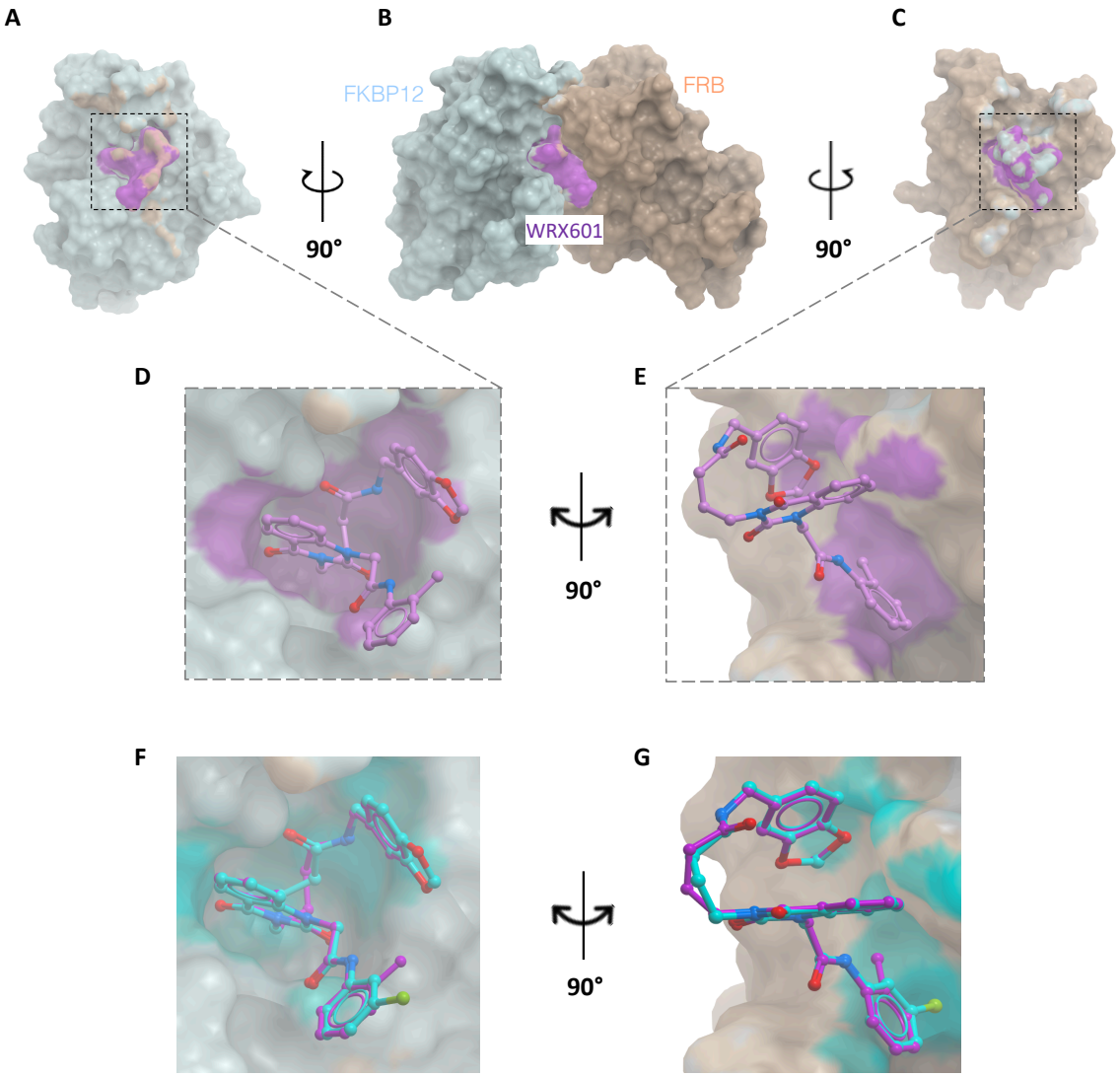

Figure S6. FKBP12–WRX601–FRB ternary complex. (A) Molecular surface representation of **WRX601** (purple) at the FKBP12 binding site (light blue). (B) Lateral view of FKBP12–**WRX601**–FRB ternary complex. (C) **WRX606** in the FRB (buff) binding site. (D) Close-up view of **WRX601** at the FKBP12 binding cleft. (E) Close-up view of **WRX601** at the FRB binding cleft. (F) Superposed view of **WRX601** (purple) and **WRX606** (cyan) in the ligand-binding site of FKBP12. (G) Superposed view of **WRX601** and **WRX606** in the ligand-binding site of FRB with RMSD value of 0.82 Å.

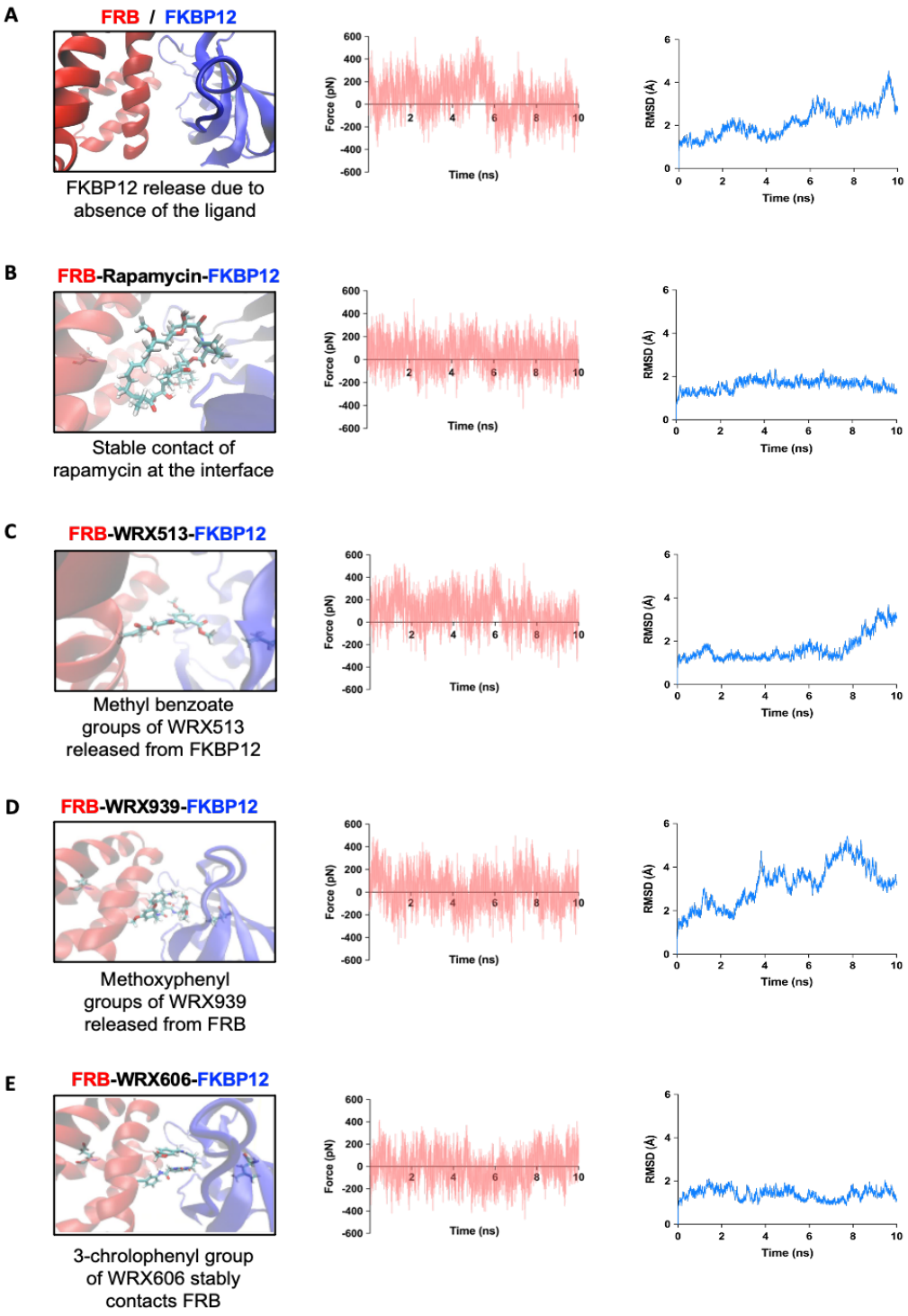

Figure S7. SMD simulations of FRB/FKBP12 complexes. SMD simulation (left) and scatter plots showing the force profile of the pulled FKBP12 (middle) and the conformational changes, represented by RMSD values, between the initial and SMD poses over time (right) of (A) FRB/FKBP12 interface without ligand, (B) FRB-rapamycin-FKBP12, (C) FRB-**WRX513**-FKBP12, (D) FRB-**WRX939**-FKBP12 and (E) FRB-**WRX606**-FKBP12. Time-course movies can be viewed in Figures S7A-E.mpg.

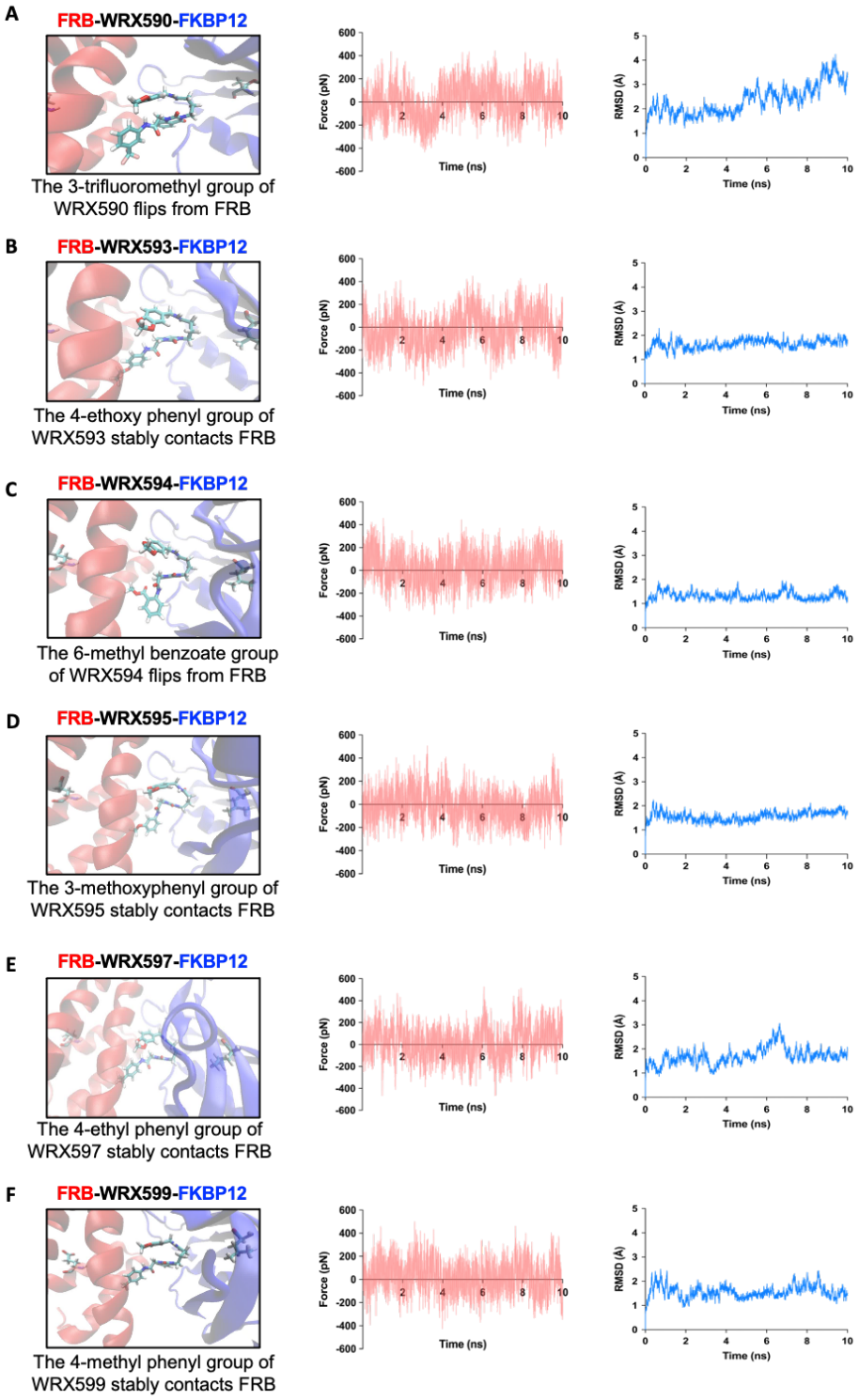

Figure S8. SMD simulations of FRB/FKBP12 complexes. SMD simulation (left) and scatter plots showing the force profile of the pulled FKBP12 (middle) and the conformational changes, represented by RMSD values, between the initial and SMD poses over time (right) of (A) FRB-**WRX590**-FKBP12, (B) FRB-**WRX593**- FKBP12, (C) FRB-**WRX594**-FKBP12, (D) FRB-**WRX595**-FKBP12, (E) FRB-**WRX597**-FKBP12 and (F) FRB- **WRX599**-FKBP12. Time-course movies can be viewed in Figures S8A-F.mpg.

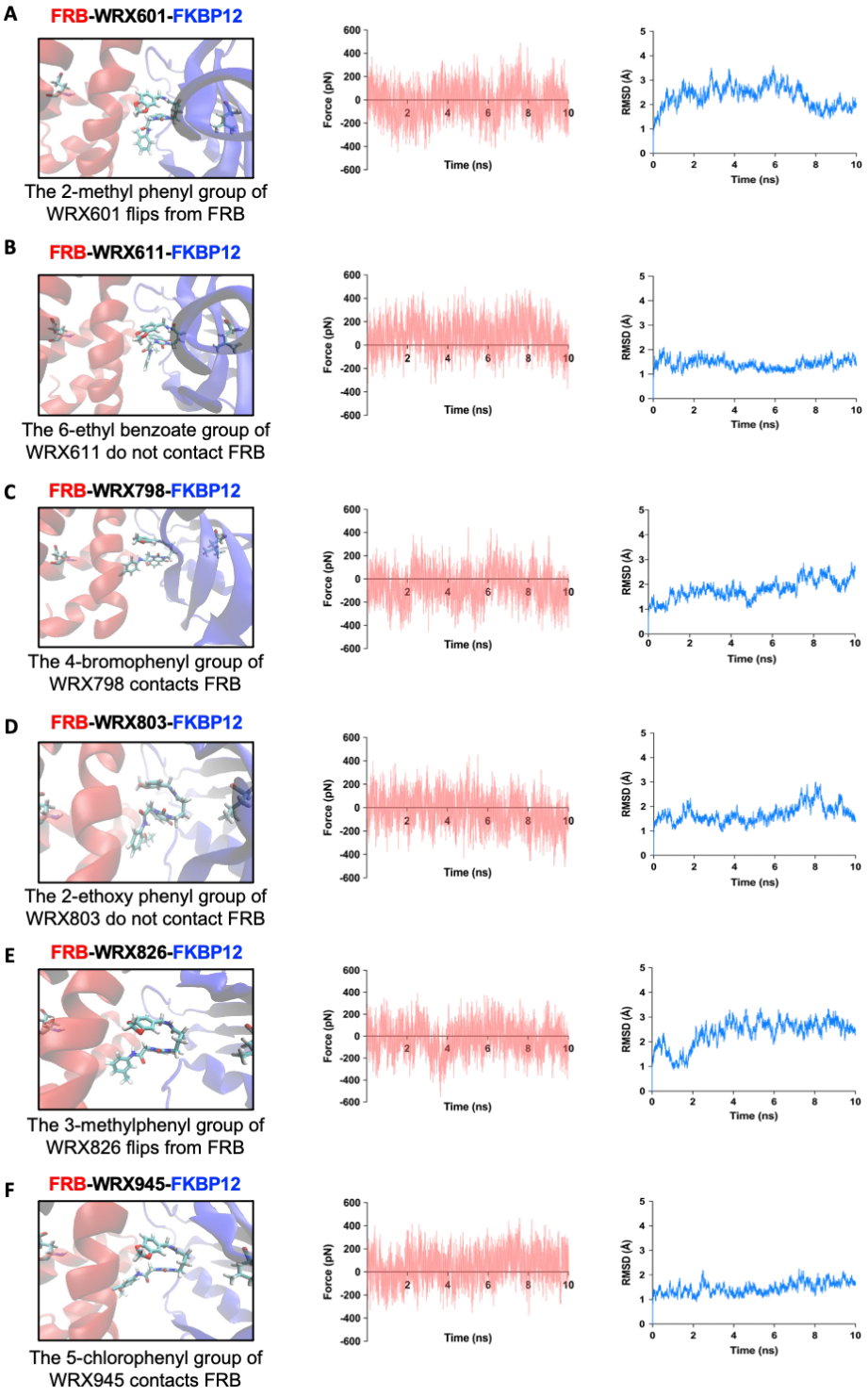

Figure S9. SMD simulations of FRB/FKBP12 complexes. SMD simulation (left) and scatter plots showing the force profile of the pulled FKBP12 (middle) and the conformational changes, represented by RMSD values, between the initial and SMD poses over time (right) of (A) FRB-**WRX601**-FKBP12, (B) FRB-**WRX611**- FKBP12, (C) FRB-**WRX798**-FKBP12, (D) FRB-**WRX803**-FKBP12, (E) FRB-**WRX826**-FKBP12 and (F) FRB- **WRX945**-FKBP12. Time-course movies can be viewed in Figures S9A-F.mpg.

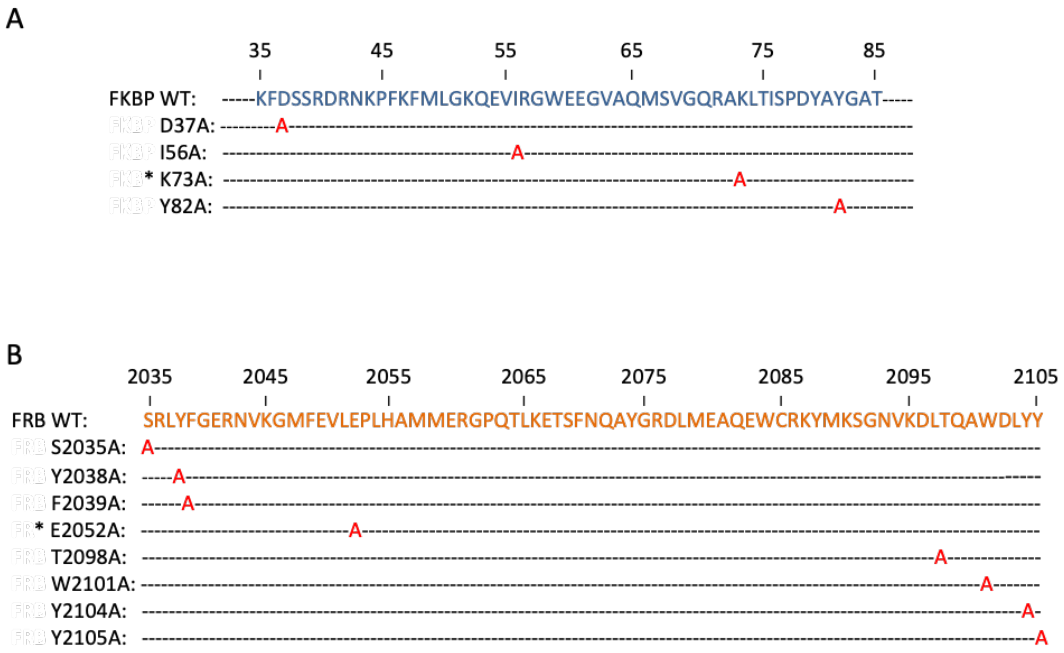

Figure S10. Sequence alignments of FKBP12 or FRB point mutants. (A) Amino acid sequences involved in the ligand-binding region of FKBP12. (B) Amino acid sequences involved in the ligand-binding region of FRB shown as wild type or mutant variants as indicated. All indicated residues were mutated to alanine (highlighted in red color). Asterisks identify negative control residues located away from the binding site.

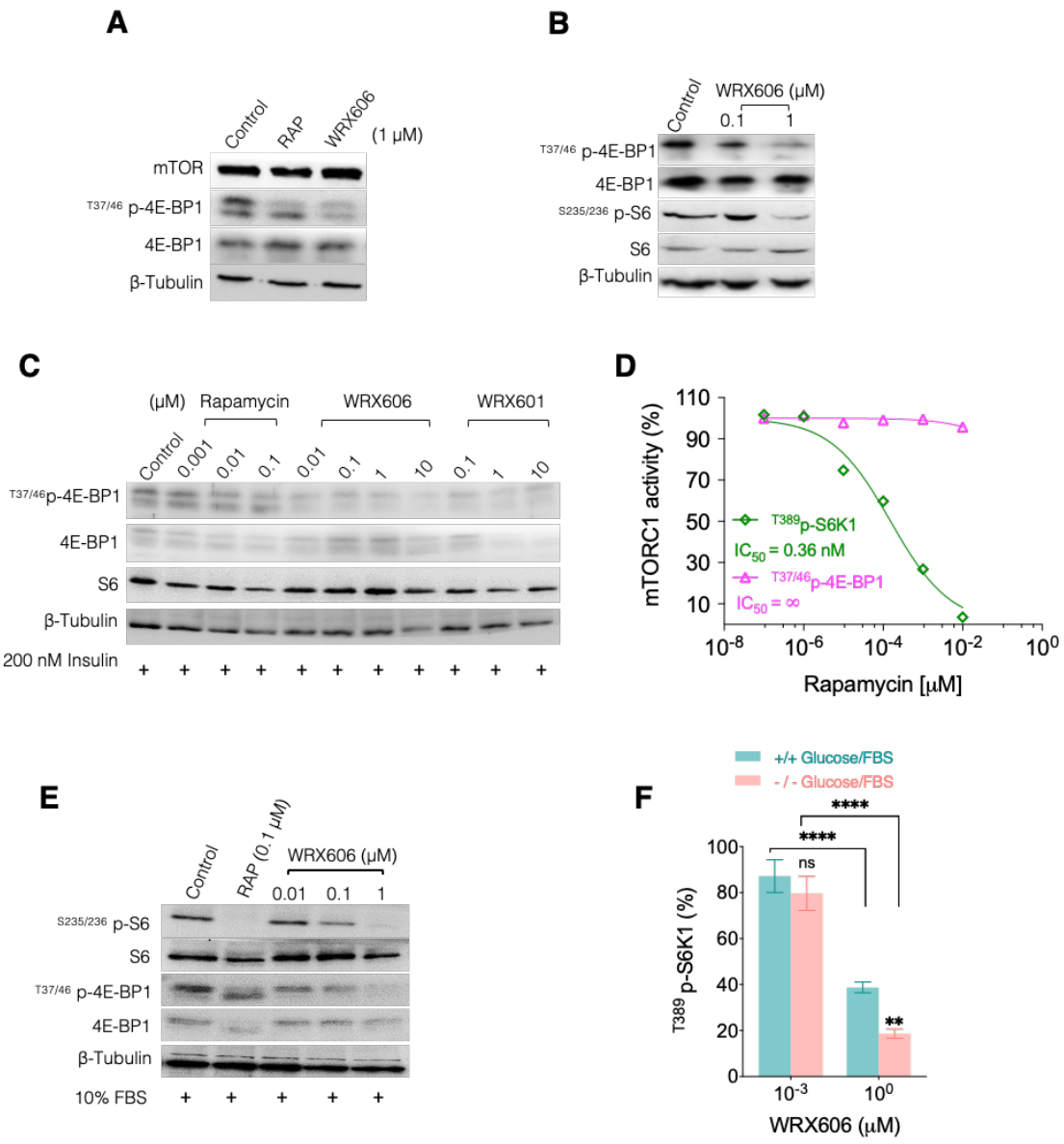

Figure S11. Inhibition of mTORC1 by WRX606. (A) Western blot analysis of $^{T37/46}$p-4E-BP1 signal of serum-starved HeLa cells treated with **WRX606** or rapamycin for 3h. (B) Western blot analysis of mTORC1 downstream signals of serum-starved HeLa cells treated with different concentrations of **WRX606** for 3h. (C) Western blot analysis of mTORC1 downstream signals of MCF-7 cells under insulin-dependent mTORC1 activation treated with different concentrations of rapamycin, **WRX606,** or **WRX601** for 6h. Insulin (200 nM) was added 1 h before cell lysis. (D) Evaluation of mTORC1 kinase activity of prestarved HeLa cells treated with increasing rapamycin concentrations for 6h after insulin stimulation (200 nM) for 1h. The results are indicated as percent of control (n = 1), shown as representative of two independent experiments. (E) Western blot analysis of mTORC1 downstream signals of A549 cells under feeding conditions treated with different concentrations of **WRX606** or rapamycin. Experimental data are representative of two independent experiments each. (F) Evaluation of increasing concentrations of **WRX606** on mTORC1 kinase activity in serum-starved or nourished HeLa cells for 3h, the results are indicated as percent of control (GLU; glucose; FBS: fetal bovine serum) (mean ± SD; n = 3). Two-way ANOVA was used: ****P < 0.0001 ; **P < 0.01; ns, P > 0.05.

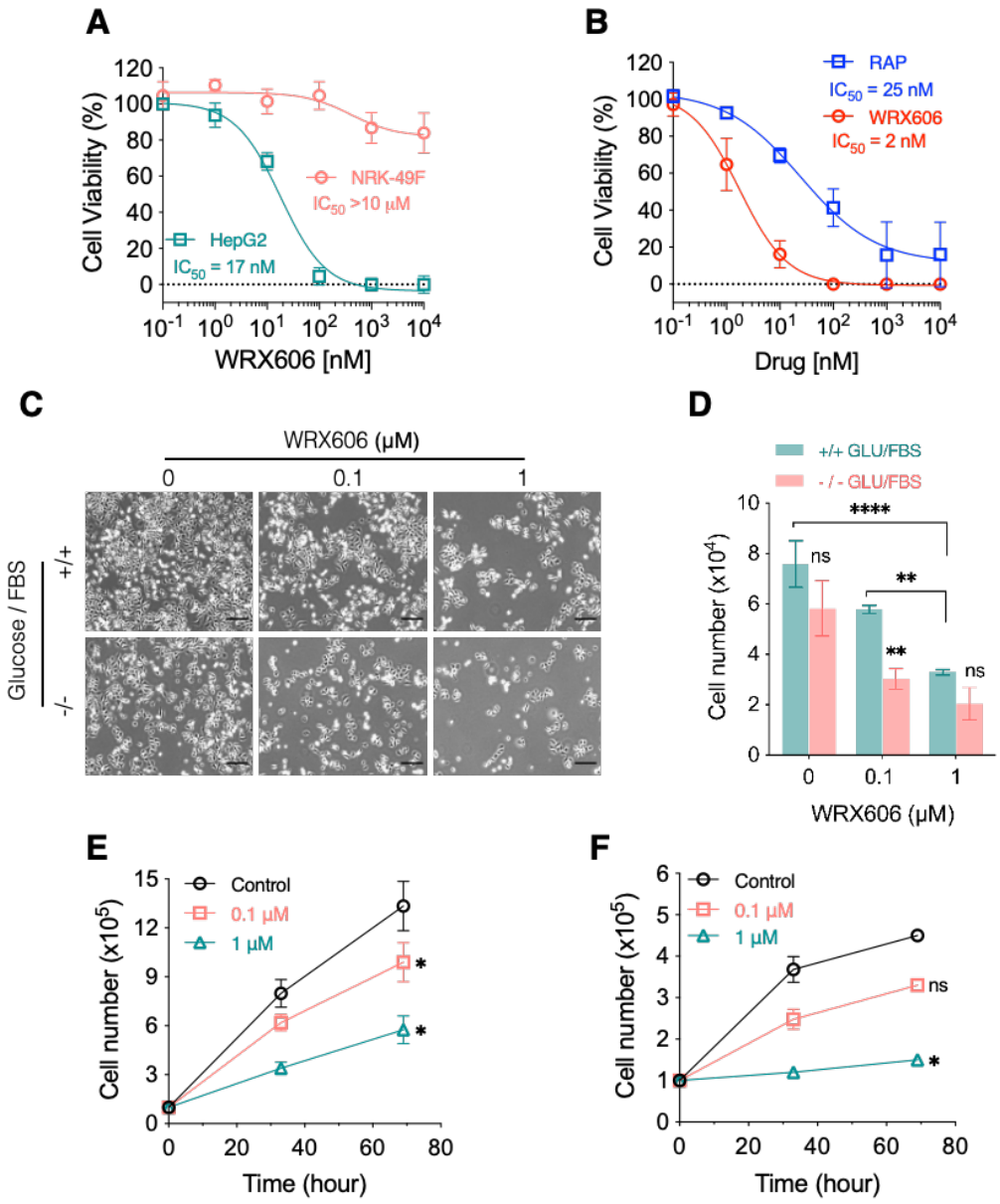

Figure S12. Cytotoxicity of WRX606 under feeding-induced activation conditions. (A) Cell viability of cancer (HepG2) and noncancer (NRK-49F) cell lines treated with increasing concentrations of **WRX606** for 72 h under serum-starved conditions using CellTitre-Blue assay kit (mean ± SD; n = 3). (B) Comparison of the effects of increasing concentrations of **WRX606** or rapamycin in serum-starved HeLa cells (mean ± SD; n = 3). (C) Evaluation of the dose-dependent effect of **WRX606** on HeLa cell line for 48 h under mTORC1-feeding activation or serum-starved conditions using the trypan blue quantification method (mean ± SD; n = 3). Images were analyzed using ImageJ software (scale bar: 100 µm). (D) Quantitative assays of (C). Data are representative of two independent experiments. (E) Proliferation curves of HeLa cells treated with increasing concentrations of **WRX606** over 69 h under feeding-induced activation conditions. (F) Proliferation curves of HeLa cells treated with increasing concentrations of **WRX606** over 69 h under starvation conditions, using trypan blue quantification method (mean ± SEM; n = 3). Data are representative of two independent experiments each. Correlation analysis or two-way ANOVA was used: ****P < 0.0001; **P < 0.01; *P < 0.05; ns, P > 0.05.

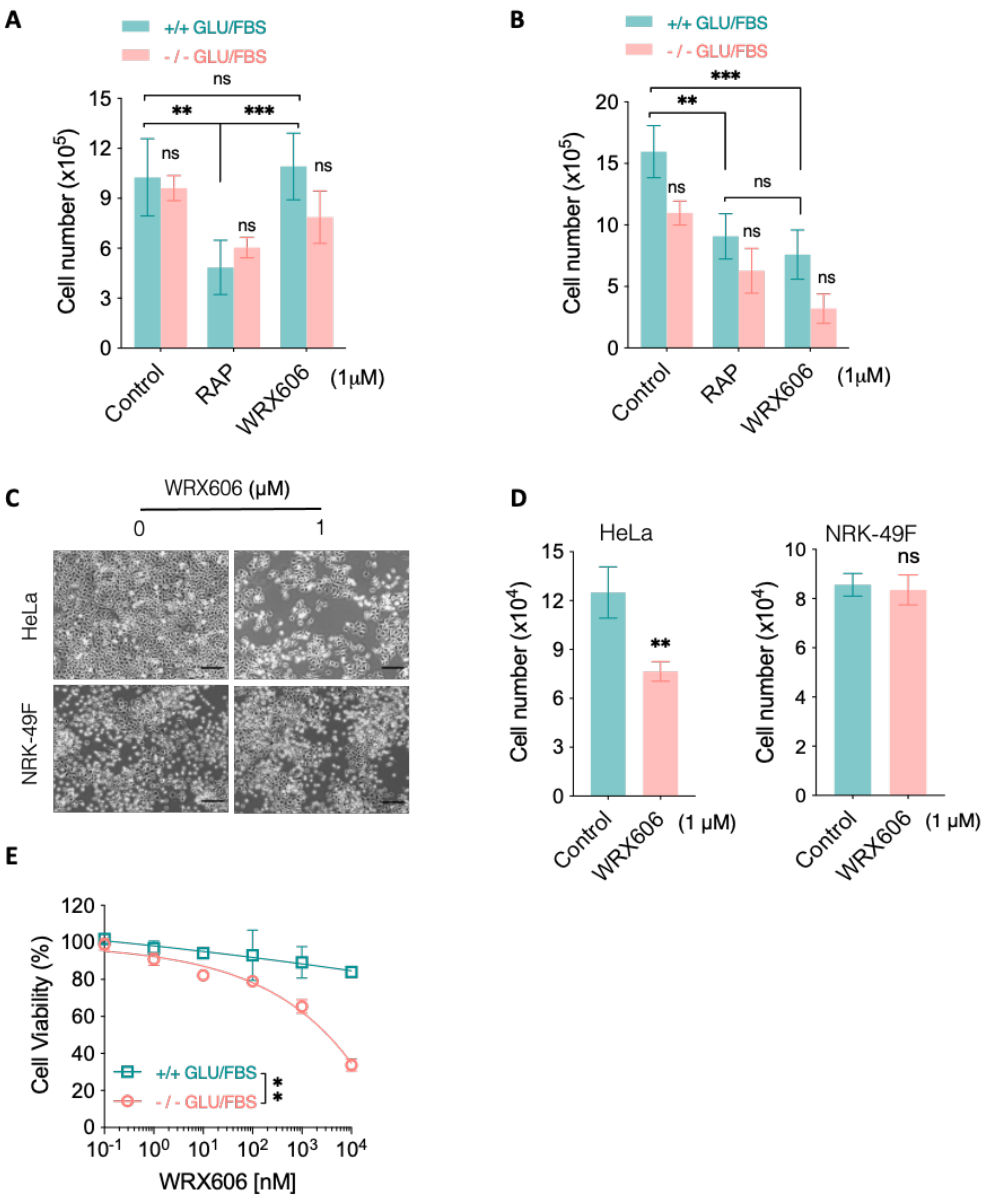

Figure S13. Cancer-specific cytotoxicity of WRX606. (A) Comparing the cytotoxic effects of 1 μM **WRX606** or rapamycin under mTORC1-dependent feeding activation or serum-starved conditions for 48 h on noncancer NRK-49F cells (mean ± SD; n = 4). (B) Cytotoxic effects of 1 μM **WRX606** or rapamycin under mTORC1-dependent feeding activation or serum-starved conditions for 48 h on cancer HeLa cells (B; mean ± SD; n = 3). Starvation was for 18 h in all experiments. (C) Comparison between the effect of **WRX606** (1 μM) on HeLa or NRK-49f cell lines under activation conditions for 48 h using trypan blue quantification method (mean ± SEM; n = 3). Images were analyzed using ImageJ software (scale bar: 100 μm). (D) Quantitative results of (C). (E) Evaluation of the dose-dependent effects of **WRX606** on HEK293 cell line under mTORC1-dependent feeding activation or serum-starved conditions (mean ± SEM; n = 3). Data are representative of two independent experiments. Correlation analysis and one-way or two-way ANOVA were used: ***P < 0.001; **P < 0.01; ns, P > 0.05.

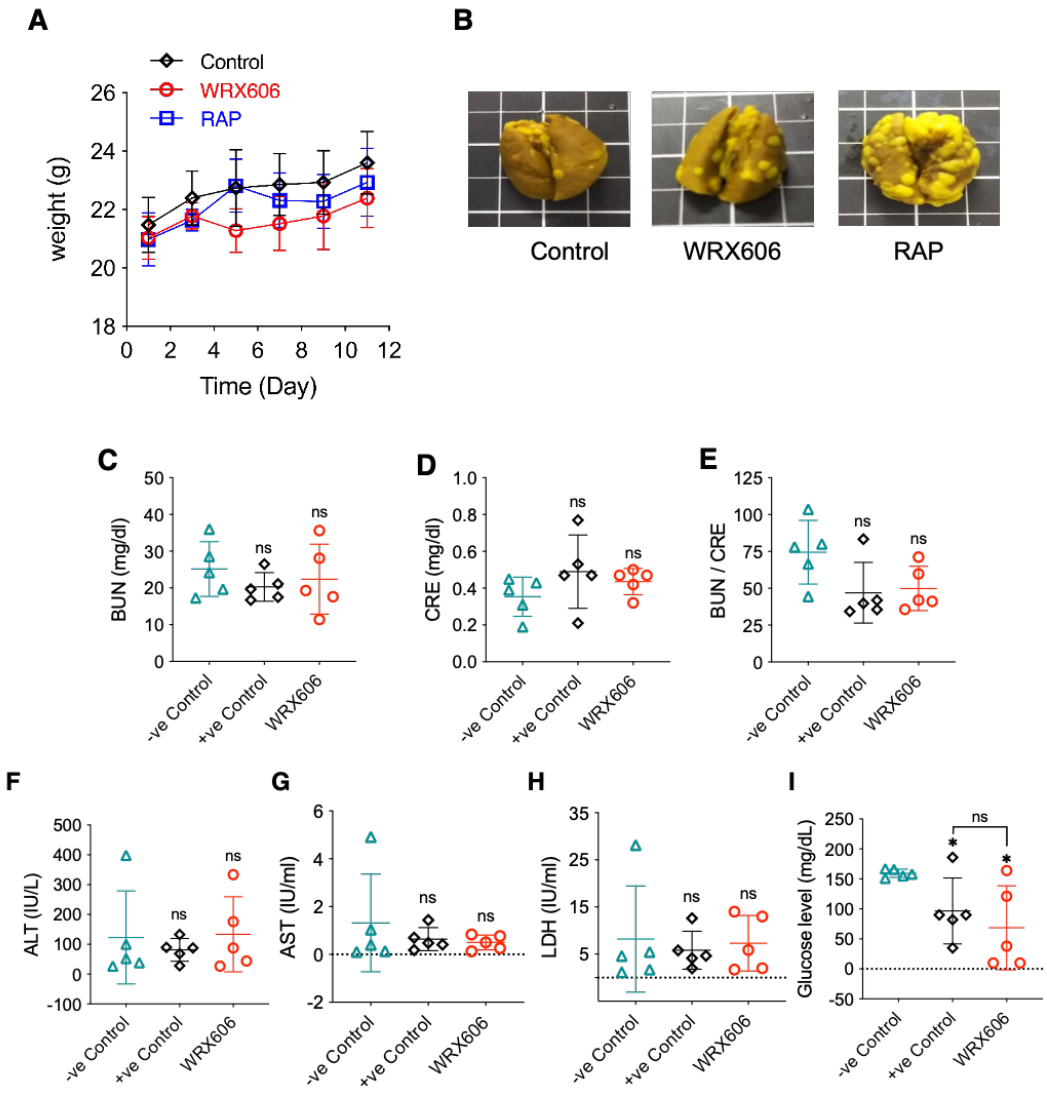

Figure S14. Animal experiments to assay metastasis and toxicity of WRX606 to organs. (A) Weights of mice in the treated and control groups during the experiment. (B) Metastatic behavior of 4T1 cells in the different treated groups. Metastatic colonies in the mouse lungs are shown in whitish-yellow color. (C–I) Evaluation of the effect of **WRX606** on the blood profile of treated mice with reference to positive control group (nontreated tumor model) and negative control group (nontreated, nontumor model). (C) Evaluation of blood urea nitrogen (BUN) levels. (D) Evaluation of blood creatinine (CRE) levels. (E) Kidney function indicated by BUN/CRE ratio. (F) Evaluation of liver function determined by blood levels of alanine transaminase (ALT). (G) Blood levels of aspartate transaminase (AST). (H) Evaluation of the possibility of tissue damage determined by the levels of lactate dehydrogenase (LDH). (I) Evaluation of serum glucose levels. Data represent mean ± SD (n = 5). Unpaired t-test was used: *P < 0.05; ns, P > 0.05.

Table S1. Residual interactions of FRB and FKBP12 with rapamycin (Figure S1)

Protein	Residue	Bond type	Ligand atom	Distance (Å) *
FKBP12	I56	Hydrogen bond	o2	2.78
	Y82	Hydrogen bond	o3	2.71
	D37	Hydrogen bond	o6	2.76
	E54	Hydrogen bond	o10	2.88
	Q53	Hydrogen bond	o13	2.62
	Y26	Hydrophobic	c5	3.73
	F36	Hydrophobic	c43	3.93
	F46	Hydrophobic	c4	3.68
	V55	Hydrophobic	c4	3.85
	W59	Hydrophobic	c3	3.41
	H87	Hydrophobic	c12	4.09
	I90	Hydrophobic	c43	3.58
	I91	Hydrophobic	c43	3.72
	F99	Vander Wal	o3	3.62
FRB	L2031	Hydrophobic	c45	3.91
	E2032	Hydrophobic	c45	4.08
	S2035	Hydrophobic	c22	3.65
	R2036	Hydrophobic	c51	3.97
	F2039	Hydrophobic	c49	3.29
	G2040	Hydrophobic	c52	3.93
	T2098	Hydrophobic	c50	4.01
	W2101	Hydrophobic	c20	3.62
	D2102	Hydrophobic	c50	4.05
	Y2105	Hydrophobic	c21	3.21
	F2108	Hydrophobic	c45	3.43

* Distance between the ligand atom and the residue.

Table S2. Characteristics of virtual ligands libraries

Parameters	1st library (L#1)	2nd library (L#2)	3rd library (L#3)
Availability	In-stock	In-stock	In-stock
Molecular weight (Da)	200–250	450–500	>500
logP	−1: 3	−1: 3	−1: 4
Reactivity	Standard	Standard	Standard
Representation	3D	3D	3D
Charge	Neutral	Neutral	Neutral
pH	7.4	7.4	7.4
Total ligand number	304,417	200,000	155,000

Table S3. Docking and SMD results of the selected ligands

Molecule	Molecular weight (Da)	LogP	Docking score	Hydrogen bonding (kcal/mol)	Hydrophobic interaction (kcal/mol)	ΔG FKBP12/FRB (kcal/mol)	SMD RMSD± SD (Å)
Rapamycin	914.20	5.24	−46.50*	−6.27	−15.64	−12.60	1.61 ± 0.26
WRX513	468.40	0.91	−39.40	−2.98	−5.54	−6.18	1.65 ± 0.59
WRX939	575.70	3.83	−44.60	−6.11	−10.39	−6.96	3.18 ± 0.97
WRX606	549.00	3.28	−41.45	−7.27	−9.23	−5.72	1.39 ± 0.25
WRX590	582.53	3.65	−33.70	−5.30	−9.93	−4.57	2.35 ± 0.60
WRX593	558.60	3.03	−29.90	−5.28	−9.49	−2.69	1.65 ± 0.19
WRX594	572.57	2.41	−35.97	−5.26	−9.02	−3.44	1.32 ± 0.17
WRX595	544.56	2.64	−35.60	−5.28	−9.13	−3.24	1.57 ± 0.19
WRX597	542.53	3.19	−38.93	−5.31	−9.46	−3.93	1.70 ± 0.35
WRX599	528.56	2.94	−32.73	−5.25	−9.37	−3.94	1.56 ± 0.26
WRX601	528.56	2.94	−31.09	−5.32	−9.41	−3.14	2.34 ± 0.45
WRX611	586.60	2.80	−34.00	−5.28	−9.49	−2.60	1.42 ± 0.20
WRX798	611.42	3.53	−38.70	−5.30	−9.61	−5.61	1.80 ± 0.39
WRX803	558.60	3.03	−17.73	−6.24	−9.61	−3.23	1.69 ± 0.36
WRX826	528.56	2.94	−29.87	−5.28	−9.55	−3.92	2.36 ± 0.54
WRX945	579.00	3.29	−21.62	−3.62	−9.59	−4.55	1.47 ± 0.24

*Redocking binding score.

Table S4. Interactions of FRB and FKBP12 with WRX606 (Figures 1H–K)

Protein	Residue	Bond type	Ligand atom	Distance (Å) *
FKBP12	Y82	Hydrogen bond	o1	2.51
	D37	Hydrogen bond	n1	3.27
	I56	Hydrogen bond	o5	2.74
	Y26	Hydrophobic	c1	3.94
	F36	Hydrophobic	c3	3.91
	F46	Hydrophobic	c12	4.22
	V55	Hydrophobic	c12	3.83
	W59	Hydrophobic	c11	3.62
	H87	Hydrophobic	c6	4.38
	I90	Hydrophobic	c3	4.21
	F99	Hydrophobic	c1	3.66
FRB	S2035	Hydrophobic	c26	4.36
	F2039	Hydrophobic	c10	3.70
	T2098	Hydrophobic	c10	3.82
	W2101	Hydrophobic	Cl1	1.95
	Y2104	Hydrophobic	Cl1	3.81
	Y2105	Hydrophobic	c27	3.43

* Distance between the ligand atom and the residue.

Table S5. Interactions of FRB and FKBP12 with WRX513 (Figures S4A–C)

Protein	Residue	Bond type	Ligand atom	Distance (Å) *
FKBP12	I56	Hydrogen bond	o3	2.95
	F46	Hydrophobic	c7	4.17
	V55	Hydrophobic	c7	3.83
	W59	Hydrophobic	c7	4.05
FRB	S2035	Hydrogen bond	n2	2.93
	L2031	Hydrophobic	c16	4.41
	E2032	Hydrophobic	c18	3.91
	F2039	Hydrophobic	c10	3.81
	G2040	Hydrophobic	c1	3.85
	W2101	Hydrophobic	c16	4.15
	Y2105	Hydrophobic	c12	4.15
	F2108	Hydrophobic	c16	3.34

* Distance between the ligand atom and the residue.

Table S6. Interactions of FRB and FKBP12 with WRX939 (Figures S4D–F)

Protein	Residue	Bond type	Ligand atom	Distance (Å) *
FKBP12	Y82	Hydrogen bond	n1	2.76
	E54	Hydrogen bond	n2	3.28
	I56	Hydrogen bond	o5	2.66
	Y26	Hydrophobic	c27	3.63
	F36	Hydrophobic	c32	3.95
	D37	Hydrophobic	c28	4.02
	F46	Hydrophobic	c13	4.01
	V55	Hydrophobic	c24	3.55
	W59	Hydrophobic	c31	3.09
	H87	Hydrophobic	c1	4.32
	I91	Hydrophobic	c1	3.33
	L97	Hydrophobic	c32	4.00
	F99	Hydrophobic	c32	0.44
FRB	S2035	Hydrophobic	c21	4.03
	F2039	Hydrophobic	c6	2.84
	T2098	Hydrophobic	c4	3.79
	W2101	Hydrophobic	c17	4.17
	Y2105	Hydrophobic	c17	3.78
	F2108	Hydrophobic	c21	3.56

* Distance between the ligand atom and the residue.

Table S7. Interactions of FRB and FKBP12 with WRX601 (Figures 2D–G)

Protein	Residue	Bond type	Ligand atom	Distance (Å) *
FKBP12	I56	Hydrogen bond	o3	2.78
	Y82	Hydrogen bond	o4	2.41
	Y26	Hydrophobic	c19	3.97
	F36	Hydrophobic	c22	3.93
	F46	Hydrophobic	c18	4.27
	V55	Hydrophobic	c18	3.99
	W59	Hydrophobic	c19	3.86
	H87	Hydrophobic	c25	4.42
	I90	Hydrophobic	c24	4.28
	F99	Hydrophobic	c20	3.24
	D37	Van der Waals	n4	3.39
	E54	Van der Waals	c13	4.22
FRB	S2035	Hydrophobic	c4	4.46
	F2039	Hydrophobic	c25	3.72
	T2098	Hydrophobic	c26	3.88
	W2101	Hydrophobic	c1	3.45
	Y2105	Hydrophobic	c4	3.43

* Distance between the ligand atom and the residue.